Nanoscale

RSC Publishing

PAPER

CoO–carbon nanofiber networks prepared by electrospinning as binder-free anode materials for lithium-ion batteries with enhanced properties†

Cite this: *Nanoscale*, 2013, **5**, 12342

Ming Zhang,[ab] Evan Uchaker,[a] Shan Hu,[a] Qifeng Zhang,[a] Taihong Wang,*[a] Guozhong Cao*[b] and Jiangyu Li[c]

CoO_x–carbon nanofiber networks were prepared from cobalt(II) acetate and polyacrylonitrile by an electrospinning method followed by thermal treatment. The XPS results demonstrated that the cobalt compound in CoO_x–carbon obtained at 650 °C was CoO rather than Co or Co_3O_4. The CoO nanoparticles with diameters of about 8 nm were homogeneously distributed in the matrix of the nanofibers with diameters of 200 nm. As binder-free anodes for lithium-ion batteries, the discharge capacities of such CoO–carbon (CoO–C) composite nanofiber networks increased with the pyrolysis and annealing temperature, and the highest value was 633 mA h g^{-1} after 52 cycles at a current density of 0.1 A g^{-1} when the CoO–C was obtained at 650 °C. In addition, the rate capacities of the CoO–C obtained at 650 °C were found to be higher than that of the sample annealed at a lower temperature and pure carbon nanofiber networks annealed at 650 °C. The improved properties of CoO–C nanofiber networks were ascribed to nanofibers as the framework to keep the structural stability, and favorable mass and charge transport. The present study may provide a new strategy for the synthesis of binder-free anodes for lithium-ion batteries with excellent properties.

Received 29th July 2013
Accepted 3rd October 2013

DOI: 10.1039/c3nr03931e

www.rsc.org/nanoscale

Introduction

As the portable devices become increasingly thinner and lighter, there is an imperative demand for lithium-ion batteries' (LIBs) electrode materials with high specific capacity and good cyclic stability. As a typical anode material for LIBs, carbon showed satisfactory cyclic performance owing to its stable solid electrolyte interface (SEI) films and good conductance.[1] However, its specific capacity is relatively low, 372 mA h g^{-1}, based on the formation of LiC_6.[2] Preparing composites of carbon and other electrode materials is an effective strategy to achieve anode materials with enhanced specific capacity and good cyclic stability.[3–8] One case in point is that silicon with a theoretical capacity of 4400 mA h g^{-1} was employed to prepare Si/C composites,[9–13] which displayed improved reversible specific capacity towards the storage of Li^+. When the ratio of Si in composites was controlled to an appropriate value, the composites could deliver a high capacity with a good cyclic performance. However, the synthesis of such composites usually needs sophisticated processes and/or toxic chemicals, including chemical vapor deposition and silane.[10] Therefore, it is necessary to develop facile and environmentally friendly approaches to synthesize carbon-based composites with good properties for the storage of Li^+. Previous studies on cobalt–carbon composites have demonstrated that they are good candidates as anodes for LIBs with good performance.[14–21] For example, Co_3O_4–graphene composites with homogeneous distribution of Co_3O_4 showed large reversible capacity, excellent cyclic performance, and good rate capacity.[14–19,21] Cobalt–carbon composites also were prepared by electrospinning, and showed high reversible capacity and good rate capability.[17,19] However, more efforts should be made to improve the synthesis and to get a better fundamental understanding of the mechanism of the improved properties of composites.

It is well known that porous materials as electrode materials for LIBs are of benefit for enlarging the interface between electrodes and electrolyte, the transformation of Li^+, and show improved performance.[22–28] Binder and the electrical conducting carbon were commonly used to prepare electrodes,[24] resulting in the time-consuming and high cost procedure, and the transport of the electrons and Li^+ may be blocked. A possible way to circumvent these issues is to make binder-free electrode films composed of nanofibers with good conductance.[29]

[a]*Key Laboratory for Micro-Nano Optoelectronic Devices of Ministry of Education, State Key Laboratory for Chemo/Biosensing and Chemometrics, Hunan University, Changsha, 410082, P.R. China. E-mail: thwang@hnu.edu.cn; Fax: +86 731 88822332; Tel: +86 731 88822332*

[b]*Department of Materials Science & Engineering, University of Washington, Seattle, Washington, 98195, USA. E-mail: gzcao@u.washington.edu; Fax: +1 206 543 3100; Tel: +1 206 616 9084*

[c]*Department of Mechanical Engineering, University of Washington, Seattle, Washington 98195-2600, USA*

† Electronic supplementary information (ESI) available. See DOI: 10.1039/c3nr03931e

Electrospinning could be employed to prepare the binder-free electrodes.[30,31] Firstly, nanofibers arising from electrospinning could be woven into a network. Secondly, the polymer additives for electrospinning, such as polyacrylonitrile (PAN), could be readily carbonized to form a carbon fiber network with high electrical conductivity. Thirdly, the network composed of nanofibers could enlarge the interface between active materials and electrolyte, and shorten the diffusion distance of Li^+.

In this study, electrospinning was employed to conveniently prepare PAN–cobalt acetate nanofiber films. After carbonization of PAN and the decomposition of cobalt acetate at a high temperature, the composite network composed of CoO_x–carbon nanofibers was achieved. Owing to the high theoretical specific capacity of CoO_x,[32] good stability, and excellent transport properties of carbon, the composite networks as binder-free anodes showed high reversible capacity and excellent cyclic performance at a high rate. The effects of temperature for thermal treatment on the electrochemical properties of the networks were investigated in detail.

Experimental section

Cobalt(II) acetate tetrahydrate ($Co(CH_3COO)_2 \cdot 4H_2O$, Alfa Aesar Co., Ltd., USA), polyacrylonitrile (PAN, $M_w = 150\,000$, Sigma-Aldrich Co., Ltd., USA), and *N*,*N*-dimethylformamide (NMP, J. T. Baker Co., Ltd., USA) were purchased and used without any purification. To prepare the precursor solution, PAN and $Co(CH_3COO)_2 \cdot 4H_2O$ were dissolved in DMF to form solutions with concentrations of 6.5 wt% and 2.5 wt%. To prepare pure carbon fibers, the precursor without cobalt acetate also was prepared. Then the solution was transferred into a 3 mL syringe with a stainless steel needle (0.6 mm inner diameter). A syringe pump controlled the flow rate of the precursor solution to about 0.4 mL h^{-1}. An aluminum foil as the collector was vertically positioned at 15 cm away from the needle. The needle was connected to a high voltage DC power to get a voltage of 14–18 kV. Under these conditions, pure PAN fibers and PAN–cobalt acetate fibers were generated and formed the films of networks. After being pre-oxidized at 225 °C in air for 6 h, the resulting brown films were treated at 550–650 °C in nitrogen for 2 h to carbonize the PAN and decompose the cobalt acetate. The products were marked as CoO_x–C. The pure PAN fibers were treated in the same way to obtain carbon fibers.

The samples were characterized by powder X-ray diffraction (XRD) on a D8 Bruker X-ray diffractometer with Cu K_α irradiation ($\lambda = 0.15406$ nm). The microstructure and morphology of the composites were analyzed using a JEOL JSM-7000F scanning electron microscope (SEM), and a FEI Tecnai G2 F20 transmission electron microscope (TEM) operating at 200 kV accelerating voltage. Elemental analysis of samples was achieved using energy dispersive spectroscopy (EDS). Thermogravimetric analysis (TGA) data were collected on a Netzsch STA449C. The crystalline phase of the samples also was detected by X-ray photoelectron spectroscopy (XPS, Surface Science Instruments S-probe spectrometer). The binding energy scales were calibrated by assigning the lowest binding energy C1s peak a binding energy of 285.0 eV.

The CoO_x–C nanofiber networks and pure carbon nanofiber networks were directly used as binder-free anodes for electrochemical measurements towards the storage of Li^+. A Celgard 2400 microporous polypropylene membrane was used as a separator. The electrolyte consisted of a solution of 1 M $LiPF_6$ in ethylene carbonate–dimethyl carbonate (1 : 1, in volume). Pure lithium foils were used as the counter and reference electrodes. These cells were assembled in an argon-filled glove-box with the moisture and oxygen levels less than 1 ppm. The discharge and charge measurements were carried out using an Arbin BT2000 system with the cut off potentials being 0 V for discharge and 3 V for charge. The specific capacities were calculated based on the weight of the composites. The cyclic voltammetry results were collected on the electrochemical workstation (CHI660B). After the cyclic test, the coin cell was unassembled in the glove-box, and the electrode was rinsed with dimethyl carbonate and acetonitrile several times. After drying in a vacuum oven, it was characterized by TEM.

Results and discussion

The morphology and diameters of PAN–cobalt acetate fibers, the stabilized nanofibers, and the carbonized (650 °C) nanofiber networks were characterized by SEM with an acceleration voltage of 10 kV, and the results are shown in Fig. 1. It can be found from Fig. 1a that the as-prepared PAN–cobalt acetate fibers are randomly oriented and their lengths are more than ten micrometers. A high magnification in Fig. 1d reveals that the surface of these fibers is smooth and their diameters are distributed in the range of 190–230 nm with an average diameter of 215 nm. After stabilization in air at 225 °C (Fig. 1b), there is no appreciable distinction between the stabilized nanofibers and the as-prepared ones. The amplified image of stabilized fibers in Fig. 1e shows that their diameters are about 190 nm and they become less smooth compared with the raw fibers. The decrease of diameter could be attributed to the decomposition of PAN and the shrinkage of the fibers through partial sintering.[33] The images of carbonized PAN–cobalt acetate in Fig. 1c demonstrate that the fiber morphology is conserved. According to the enlarged image in Fig. 1f, the CoO_x–C fibers with diameters of 175 nm are rough and embedded with some nanoparticles. In comparative experiments, there was no cobalt acetate in the precursor and pure PAN nanofibers were fabricated. After processing with the same procedure as for PAN–cobalt acetate, PAN fibers were carbonized and the SEM image is shown in Fig. 1g. Those nanofibers with diameters of about 165 nm are uniform and smooth. The EDS characterization of carbonized PAN–cobalt acetate nanofibers is presented in Fig. 1h. Those results show the presence of C, O, Co and N in them, which could be assigned to cobalt oxide, carbon and the residual nitrogen from PAN.[34] The digital photo of CoO_x–C nanofiber networks is displayed in Fig. 1i. The film with a diameter of 1.2 cm is integral without any crack, showing the structural integrity of the networks and its potential application in LIBs without any binders.

In order to further elucidate the bond state of the cobalt in the CoO_x–C nanofibers, XPS analysis was carried out on a

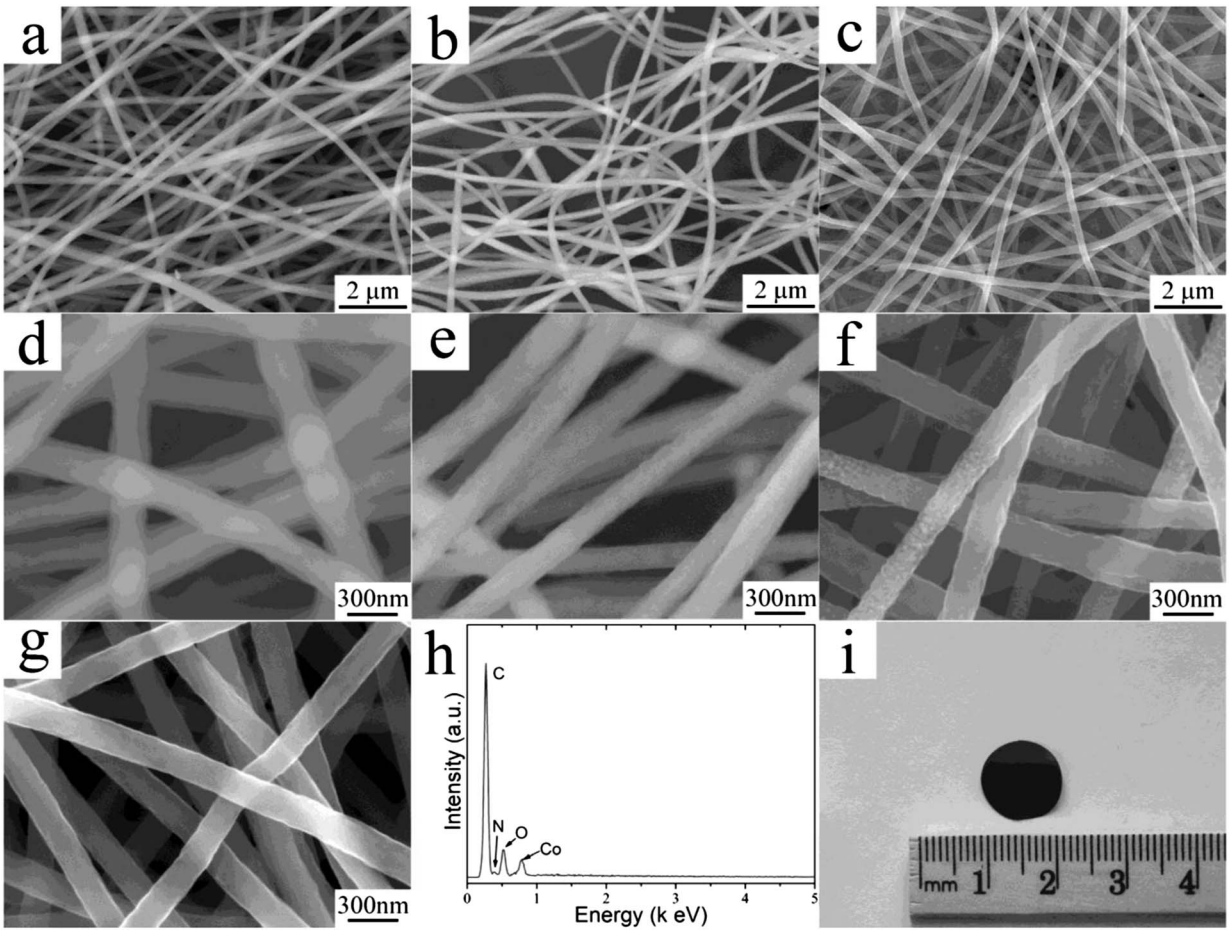

Fig. 1 (a) and (d) display the SEM images of as prepared PAN–cobalt acetate fibers; (b) and (e) show the SEM images of the pre-oxidized PAN–cobalt acetate fibers; (c), (f), and (h) present the SEM images and EDS spectra of CoO_x–C nanofibers synthesized at 650 °C; (g) the SEM images of pure carbon obtained at 650 °C; and (i) the digital photo of a binder-free anode based on CoO_x–C nanofiber networks synthesized at 650 °C.

Surface Science Instruments S-probe spectrometer. This instrument has a monochromatized Al K_α X-ray and a low energy electron flood gun for charge neutralization of non-conducting samples. The XPS spectra of CoO_x–C in Fig. 2a exhibit four main peaks at 285.0, 398.6, 531.2 and 780.5 eV, corresponding to the peaks of C 1s, N 1s, O 1s and Co $2p_{3/2}$.[35–38] These results are highly consistent with those of EDS. The Co 2p XPS spectra of CoO_x–C in Fig. 2b exhibit two peaks at 780.5 and 796.4 eV associated with two satellite peaks. The $2p_{3/2}$ peak at 780.5 eV can be assigned to Co^{2+} coordinated to oxygen anions.[36] The satellite peak arising from the occurrence of a ligand-to-metal charge transfer during the photoemission process was used as a fingerprint for the recognition of high-spin Co(II) species in CoO_x–C.[38] The peak patterns and relative intensities of Co $2p_{3/2}$ matched well with XPS spectra for well-identified CoO standards in the literature,[35,36,38] demonstrating that these samples were CoO–C composites rather than cobalt and Co_3O_4. In Fig. 2c, the peaks at 531.2 and 532.6 eV indicated the presence of oxygen-containing groups on the surface.[37,39] The O 1s peak at about 530 eV which corresponds to oxygen species in the spinel cobalt oxide phase (Co_3O_4) was not found,[40] demonstrating that the cobalt compound was CoO from another direction. The XPS patterns in Fig. 2d were assigned to the N 1s, which was the residual group of PAN. The N 1s peaks at 398.6 and 400.3 eV are assigned to pyridine-type and conjugated nitrogen.[41] Both of above nitrogen have positive effects on the storage of Li^+.[42] The fine XPS spectra of C 1s are shown in Fig. 2e. The C 1s spectra could be deconvoluted to five peaks, including peak I (285.0 eV), graphitized carbon; peak II (286.5 eV), carbon in phenolic, alcohol, ether or C=O groups; peak III (288.0 eV), carbon in carbonyl or quinine groups; peak IV (289.2 eV), carbon in carboxyl or ester groups, and peak V (290.4 eV), carbon in adsorbed CO and CO_2. These results are similar to those of a previous study about PAN-based carbon nanofibers that there are some oxygen-containing groups on the surface of the nanofibers.[43]

To evaluate the weight ratio of the CoO in CoO–C nanofibers obtained at 650 °C, TGA experiments were carried out at a heating rate of 5 °C min^{-1} in air at a flow rate of 20 mL min^{-1}, the results of which are shown in Fig. 3a. The weight loss below 90 °C could be ascribed to the elimination of absorbed/trapped water molecules. The second weight loss in the TG curve began at about 260 °C and ended at about 370 °C. The shoulder in the DTA curve at about 290 °C could be assigned to the oxidation of

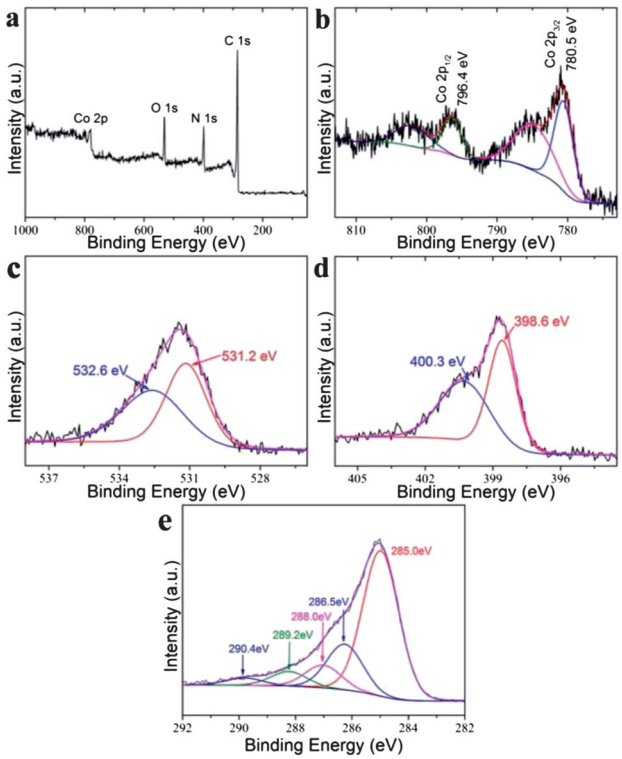

Fig. 2 (a) XPS spectrum of CoO_x–C nanofiber networks obtained at 650 °C; (b–e) the fine XPS spectra of Co 2p (b), O 1s (c), N 1s (d), and C 1s (e).

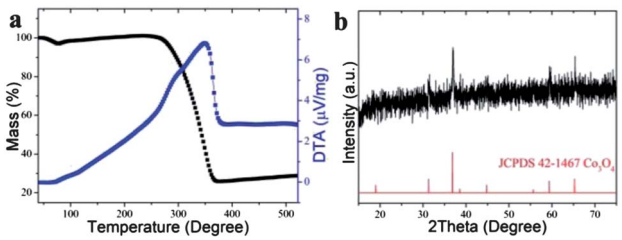

Fig. 3 (a) TG and DTA curves of CoO–C nanofibers in air and (b) the XRD patterns of the final products in the TG test.

Co^{2+}.[44] The sharp weight loss and the peak in the DTA curve at about 330 °C could be attributed to the combustion of carbon. The residue was 31.5% of the original mass. The residue of the TGA test was characterized by XRD, as shown in Fig. 3b. It is clear that the diffraction patterns and relative intensities of the final product match well with those of Co_3O_4, demonstrating that CoO in CoO–C was oxidized to Co_3O_4 during the TGA test.[45–47] Based on this mechanism, the weight ratio of CoO in the CoO–C composites was calculated to be 29.5%, and the carbon in the composites was calculated to be 70.5% in weight.

To further investigate the nanoparticles in the CoO–C composites, their TEM determinations were made, and the images are shown in Fig. 4. The TEM image at a low magnification in Fig. 4a displays that the CoO–C fibers are about 200 nm in diameter and up to several micrometers in length. The CoO nanoparticles are homogeneously distributed within the fiber. No aggregation was found. An amplified image in

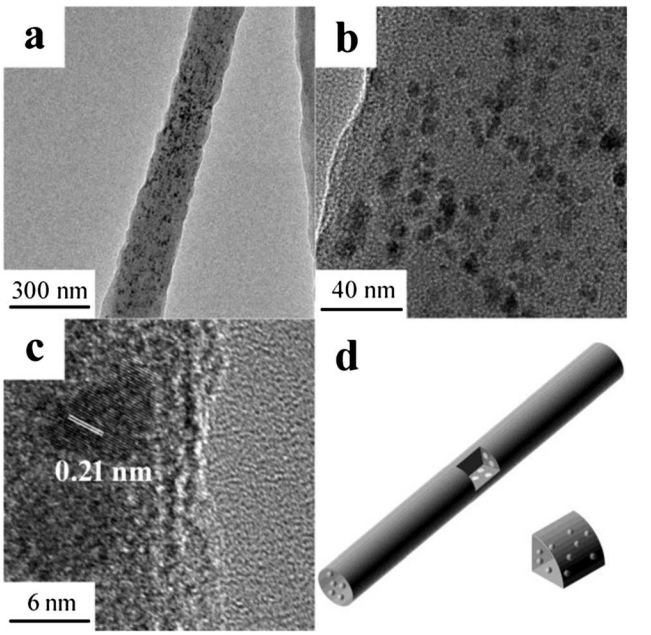

Fig. 4 (a) and (b) TEM images of CoO–C obtained at 650 °C; (c) a high resolution TEM image of the composites. The *d*-spacing of the planes was 0.21 nm; and (d) a schematic diagram showing the microstructure of CoO nanoparticles on CoO–C nanofibers.

Fig. 4b indicates that the CoO nanoparticles with diameters of about 8 nm are irregular, showing a good compatibility with carbon. The *d*-spacing of the planes in the high-resolution TEM image (Fig. 4c) is 0.21 nm, which is very close to that of the (200) plane for CoO (JCPDS 48-1719), further demonstrating that the nanoparticles are CoO. According to the above result, the microstructure of the CoO–C composites is schematically shown in Fig. 4d. The diffraction ring patterns of the SAED (now shown here) indicate the polycrystalline nature of CoO.

CV measurements were carried out over a voltage range of 0–3 V at a scan rate of 0.3 mV s^{-1} to understand the electrochemical process. The CoO–C composites prepared at 550, 600, and 650 °C were marked as C550, C600 and C650, respectively. The pure carbon fibers synthesized at 650 °C were signed as E650. In Fig. 5a and b, the cathodic peaks of C550 and C600 in the first cycle at about 1.3 V could be attributed to the electrochemical reduction reaction of CoO with Li.[18,48] Other cathodic peaks at about 0.5 and 0.7 V correspond to the formation of solid electrolyte interface (SEI) films,[18] which is the reason for the irreversible capacity loss. The broad anodic peak at about 1.1 V could be ascribed to the delithiation of carbon.[49] This peak shifts to a low potential compared with that of pure carbon fibers (Fig. 5d), which may be attributed to the active effects of cobalt on the carbon. Another anodic peak at about 2.2 V could be assigned to the oxidization of Co to CoO. The CV curves (Fig. 5c) of the sample C650 is different from those of samples C550 and C600. In the first cycle, two cathodic peaks were found at about 0.8 and 0.5 V, which could be ascribed to the lithiation of CoO and the formation of SEI films.[18] The peak potential for the lithiation of CoO in C650 is lower than those of C550 and C600, which may be attributed to the high reactivity of CoO and

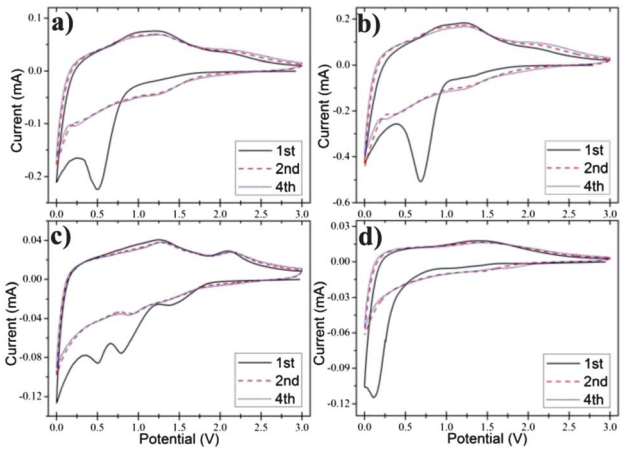

Fig. 5 CV curves of the samples C550 (a), C600 (b), C650 (c) and E650 (d) at a scan rate of 0.3 mV s^{-1}.

the improved conductance of carbon in C650. Two anodic peaks also were observed at about 1.25 and 2.15 V, which were ascribed to the delithiation of carbon and the re-oxidization of Co.[18] The intensity of the anodic peak at about 2.15 V became stronger with the increasing number of cycles. This phenomenon is different from that of pure CoO,[50] showing a positive effect of carbon on the electrochemical properties of CoO. By comparing the anodic curves at about 2.15 V, it can be found that the peak became clearer along with the increase of treating temperature. This evidence demonstrated that the activity of CoO in the sample treated at 650 °C was higher than those of samples obtained at a low temperature (550 and 600 °C). Most of the SEI films were formed in the 1st cycle, and nearly no new ones formed in the following cycles. This is the reason why there are significant changes between 1st and 2nd cycles. The curves in each image nearly overlap each other from the 2nd cycle, indicating the good cyclic stability of carbon-based electrode materials.

To investigate the effects of treatment temperature and the carbon on the electrochemical properties of CoO–C composites, five kinds (C550, C600, C650, E600, and E650) of samples were prepared. The pure carbon fibers achieved at 600 °C were labeled as E600. Fig. 6a shows the charge–discharge profiles of C650 in the 1st, 3rd, and 52nd cycles. In the 1st cycle, the C650 delivers a discharge capacity of 1112 mA h g^{-1} and a charge capacity of 798 mA h g^{-1}, corresponding to a Coulombic efficiency of 71.7%. The relatively low Coulombic efficiency could be attributed to the irreversible formation of SEI films. The discharge capacity decreases gradually from 711 mA h g^{-1} in the 3rd cycle to 633 mA h g^{-1} in the 52nd cycle. During the 1st discharge process, the plateau at about 1.1 V corresponds to the reduction of CoO and the formation of Li_2O. This plateau becomes weak in the following cycles which are similar to previous reports about CoO–C composites because of the combinative electrochemical behavior of CoO and carbon.[17,18] In the charge process, two plateaus at about 1.1 and 2.0 V could be assigned to the delithiation of carbon and the oxidation of Co to CoO. This result agrees well with the results of CVs.

Fig. 6b compares the specific capacity and cyclic properties of three samples (CoO–C) treated at different temperatures 650, 600, and 550 °C. The three samples show original discharge capacities of about 1100 mA h g^{-1}, proving their similarity. Shape decrease is found in C650, C600, and C550. However, the significant difference among them is that the discharge capacity of C650 after 52 cycles is 633 mA h g^{-1}, much higher than those of both C600 and C550. In addition, the theoretical capacity of the composites based on the mixture of PAN-based carbon (70.5 wt%, 525 mA h g^{-1} in theoretical capacity according to E650) and CoO (29.5 wt%, 715 mA h g^{-1} in theoretical capacity) could be evaluated to be 581 mA h g^{-1}, as shown in Fig. 2b (the dash line). This value is also higher than their theoretical capacities. To figure out why the sample C650 could deliver better properties, more comparative experiments were carried out, and the results are shown in Fig. 6c. The discharge capacity of E650 is about 528 mA h g^{-1} in the 4th cycle and remains at 525 mA h g^{-1} in the 52nd cycle. The discharge capacity of E600 is very close to that of E650 in the range of 4th to 52nd cycles, indicating that the effects of treating temperature on the electrochemical property of pure carbon fibers is very limited. The discharge capacity of C650 is 633 mA h g^{-1}, which is almost 1.2 times that of E650. The improved electrochemical property could be ascribed to the presence of CoO. Comparing the properties of C650, C600, C550, E650, and E600, a possible mechanism is proposed as follows. The carbon in a CoO–C composite arises from the decomposition of PAN. The properties of CoO–C composites are related to the treating temperature. The higher temperature will result in the carbon with good conductance, which is much higher than that of CoO.[51,52] Therefore the better electrochemical properties of C650 could be ascribed to the high quality of carbon to keep CoO with high properties.[33] On the other hand, the high temperature maybe results in the fibers connecting with each other very well for the fast transfer of electrons. The fast electron transport will be of benefit for keeping the electrochemical activity of CoO, resulting in a better property.

The rate capacity of CoO–C composites was compared with that of pure carbon fibers, and the results are shown in Fig. 6d. The sample C650 keeps reversible capacities of 700, 605, 505, 420, and 280 mA h g^{-1} at current densities of 0.1, 0.2, 0.5, 1, and 2 A g^{-1}, respectively. These values are higher than those of C600, showing the positive effects of the relatively high temperature on the electrochemical property of CoO–C composites. In addition, the capacity of C650 could recover to 720 mA h g^{-1} when the charge–discharge current density was brought back to 0.1 A g^{-1}, indicating the better adaptability of C650 composites. The sample C650 also showed enhanced rate capacities compared with pure carbon fibers (E650), demonstrating that the CoO particles in CoO–C composites were helpful in improving the Li^+ storage capacity of carbon fiber networks. The impedance spectra were employed to investigate the dynamic behavior, as shown in Fig. S1.† The R_e values (the resistance of the electrolyte) are almost identical in the three samples, showing the consistency of the electrolyte. The lowest R_{ct} in E650 demonstrates that its conductivity

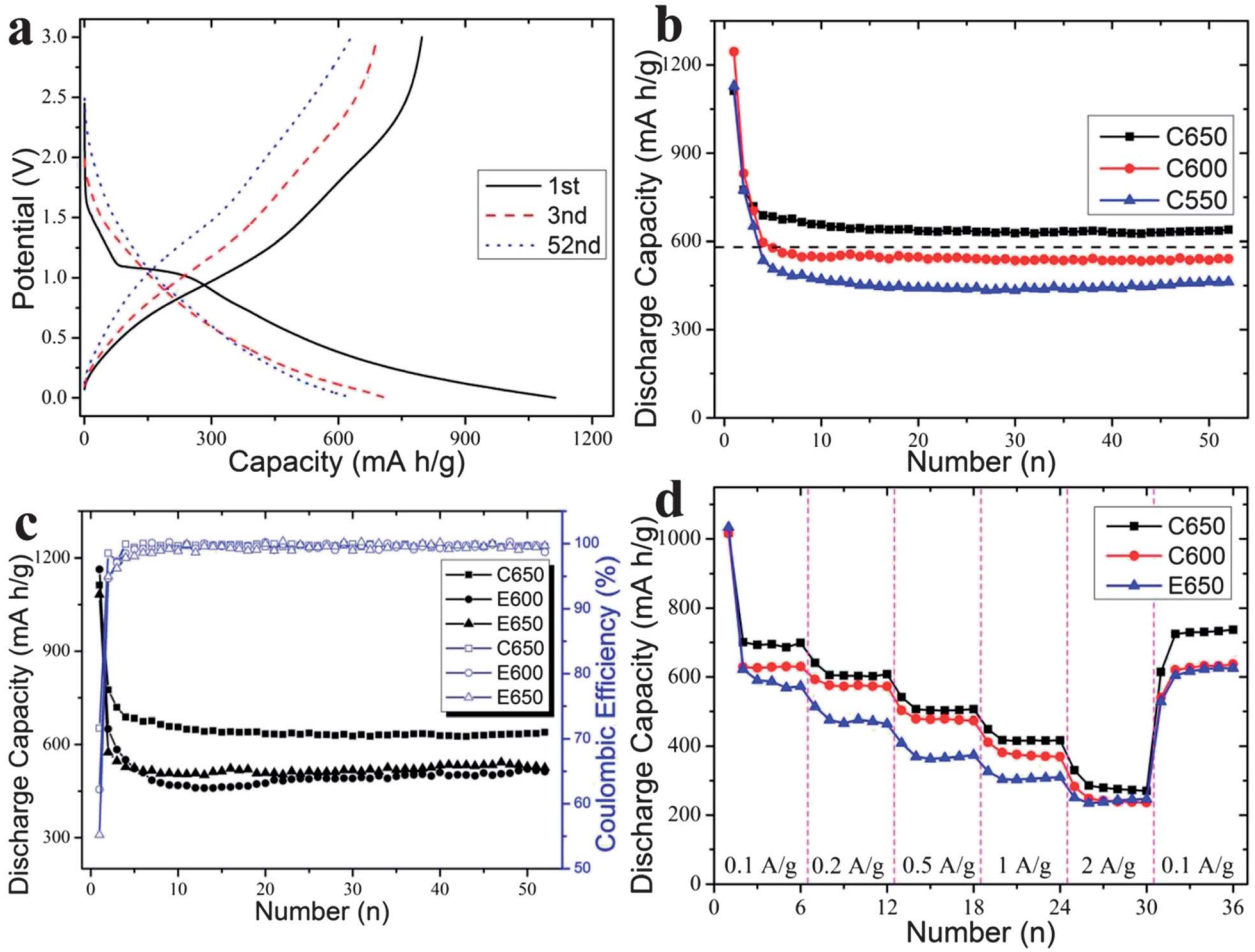

Fig. 6 (a) Discharge–charge curves of the sample C650 at a current density of 100 mA g^{-1}. (b) Cyclic properties of the samples C650, C600, and C550. (c) Specific capacities and Coulombic efficiencies of the samples C650, E650, and E600. (d) Rate capacities of the samples C650, C600, and E650.

is lower than that of CoO. Because the theoretical capacity of CoO is higher than that of carbon, the rate capacities of C650 are still higher than those of E650. The rate capacities of C650 also are higher than those of C600 because of the relatively high conductivity of C650 arising from the enhanced annealing temperature. According to above results, the improvement could be explained as follows, shown in Fig. 7. Firstly, the CoO nanoparticles were coated and connected by carbon fibers. The carbon-coating could prevent the pulverization of CoO nanoparticles and help to transport the electrons to CoO.[15] Secondly, the carbon fibers could build up to a conductive network to transfer the electrons at a high current density.[29,53] Thirdly, the binder-free anode of networks could provide more facile access of the electrolyte for active materials, and are helpful for the diffusion of Li^+.[54]

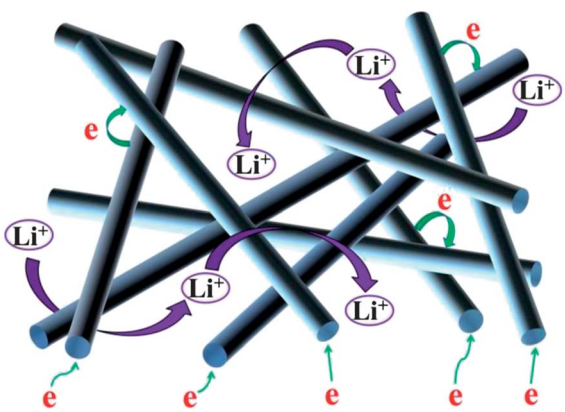

Fig. 7 A schematic representation showing that the CoO–C nanofiber networks favor the Li^+ storage.

To investigate the reason why the CoO–C networks in C650 deliver enhanced properties, they were observed by TEM after 52 cycles at a fully charged status, as shown in Fig. 8. It can be seen that the CoO–C fiber retains its original morphology with a diameter of 200 nm. The nanoparticles are clearly visible and homogeneously distributed on the fiber without any agglomeration, showing the structural integrity of the CoO–C fiber. In a high-resolution image (Fig. 8b), the clear lattice fringes are visible. The *d*-spacing of the planes is 0.246 nm, which can be indexed to the (111) plane for CoO (JCPDS 48-1719). Therefore, above results demonstrate that the Li^+ insertion and extraction process could be summarized *via* the conversion reaction of CoO ($CoO + 2Li^+ + 2e \leftrightarrow Li_2O + Co$).

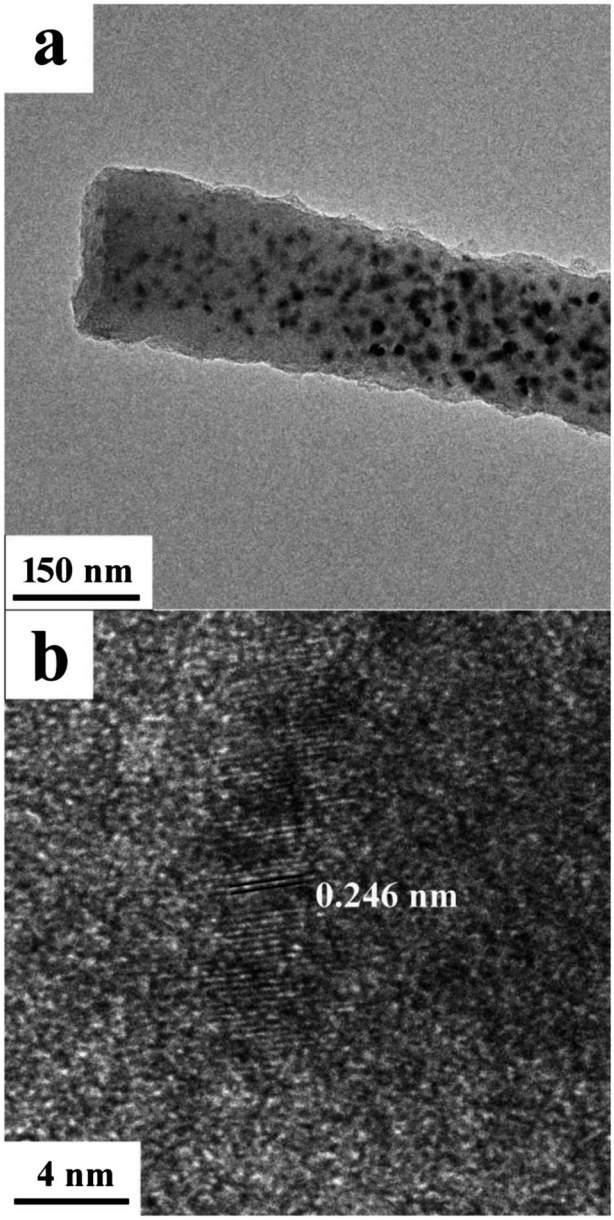

Fig. 8 TEM images at different magnification of the sample C650 after the cyclic test. The *d*–*d*-spacing of the planes was evaluated to be 0.246 nm by computing the average.

Conclusions

CoO–C nanofibers with the homogeneous distribution of CoO nanoparticles were synthesized *via* the electrospinning approach and following thermal treatment. The CoO–C nanofibers could build the network which could be used as binder-free anodes for LIBs. The networks obtained at 650 °C could deliver the discharge capacity as high as 633 mA h g^{-1} after 52 cycles at a current density of 0.1 A g^{-1}, which is higher than that of the CoO–C networks obtained at 550 and 600 °C, and the pure carbon network achieved at 600 and 650 °C. Besides, the rate capacities of CoO–C networks (650 °C) also are higher than those of CoO–C networks synthesized at 600 °C and pure carbon networks prepared at 650 °C. The improved properties could be attributed to the enhanced structural stability of CoO nanoparticles in carbon nanofibers, and improved conductance arising from the carbon nanofibers and the corresponding networks. It is believed that the strategy presented in this study will provide a new insight for the synthesis of electrodes for both LIBs and supercapacitors.

Acknowledgements

This research work has been financially supported in part by the National Science Foundation (NSF, CMMI-1030048), NESAC/BIO (EB-002027), and the University of Washington TGIF grant. Part of this work was conducted at the University of Washington NanoTech User Facility, a member of the NSF National Nanotechnology Infrastructure Network (NNIN). Ming Zhang would like to acknowledge the National Natural Science Foundation of China (61376073, 21103046), the Hunan Provincial Natural Science Foundation of China (10JJ1011 and 11JJ7004), the China Scholarship Council and Fundamental Research Funds for the Central Universities.

Notes and references

1 B. Guo, X. Wang, P. F. Fulvio, M. Chi, S. M. Mahurin, X.-G. Sun and S. Dai, *Adv. Mater.*, 2011, **23**, 4661–4666.
2 R. Kanno, Y. Takeda, T. Ichikawa, K. Nakanishi and O. Yamamoto, *J. Power Sources*, 1989, **26**, 535–543.
3 M. Zhang, D. Lei, X. Yin, L. Chen, Q. Li, Y. Wang and T. Wang, *J. Mater. Chem.*, 2010, **20**, 5538–5543.
4 J. Rong, C. Masarapu, J. Ni, Z. Zhang and B. Wei, *ACS Nano*, 2010, **4**, 4683–4690.
5 H. L. Wang, L. F. Cui, Y. A. Yang, H. S. Casalongue, J. T. Robinson, Y. Y. Liang, Y. Cui and H. J. Dai, *J. Am. Chem. Soc.*, 2010, **132**, 13978–13980.
6 L. W. Ji, Z. K. Tan, T. R. Kuykendall, S. Aloni, S. D. Xun, E. Lin, V. Battaglia and Y. G. Zhang, *Phys. Chem. Chem. Phys.*, 2011, **13**, 7139–7146.
7 X. Zhu, Y. Zhu, S. Murali, M. D. Stoller and R. S. Ruoff, *ACS Nano*, 2011, **5**, 3333–3338.
8 M. Zhang, D. Lei, Z. Du, X. Yin, L. Chen, Q. Li, Y. Wang and T. Wang, *J. Mater. Chem.*, 2011, **21**, 1673–1676.
9 L.-F. Cui, Y. Yang, C.-M. Hsu and Y. Cui, *Nano Lett.*, 2009, **9**, 3370–3374.
10 A. Magasinski, P. Dixon, B. Hertzberg, A. Kvit, J. Ayala and G. Yushin, *Nat. Mater.*, 2010, **9**, 353–358.
11 R. Yi, F. Dai, M. L. Gordin, S. Chen and D. Wang, *Adv. Energy Mater.*, 2013, **3**, 295–300.
12 J. Wang, Y. Yu, L. Gu, C. Wang, K. Tang and J. Maier, *Nanoscale*, 2013, **5**, 2647–2650.
13 S. E. Lee, H.-J. Kim, H. Kim, J. H. Park and D.-G. Choi, *Nanoscale*, 2013, **5**, 8986–8991.
14 B. J. Li, H. Q. Cao, J. Shao, G. Q. Li, M. Z. Qu and G. Yin, *Inorg. Chem.*, 2011, **50**, 1628–1632.
15 H. Qiao, L. Xiao, Z. Zheng, H. Liu, F. Jia and L. Zhang, *J. Power Sources*, 2008, **185**, 486–491.

16 J. Yue, X. Zhao and D. Xia, *Electrochem. Commun.*, 2012, **18**, 44–47.
17 W.-H. Ryu, J. Shin, J.-W. Jung and I.-D. Kim, *J. Mater. Chem. A*, 2013, **1**, 3239–3243.
18 F. Li, Q.-Q. Zou and Y.-Y. Xia, *J. Power Sources*, 2008, **177**, 546–552.
19 L. Wang, Y. Yu, P.-C. Chen and C.-H. Chen, *Scr. Mater.*, 2008, **58**, 405–408.
20 B. Das, B. Choudhury, A. Gomathi, A. K. Manna, S. K. Pati and C. N. R. Rao, *ChemPhysChem*, 2011, **12**, 937–943.
21 B. G. Choi, S.-J. Chang, Y. B. Lee, J. S. Bae, H. J. Kim and Y. S. Huh, *Nanoscale*, 2012, **4**, 5924–5930.
22 Y. S. Hu, P. Adelhelm, B. M. Smarsly, S. Hore, M. Antonietti and J. Maier, *Adv. Funct. Mater.*, 2007, **17**, 1873–1878.
23 F. Zhang, K. X. Wang, G. D. Li and J. S. Chen, *Electrochem. Commun.*, 2009, **11**, 130–133.
24 P. Adelhelm, Y. S. Hu, L. Chuenchom, M. Antonietti, B. M. Smarsly and J. Maier, *Adv. Mater.*, 2007, **19**, 4012–4017.
25 M. Zhang, Y. Li, E. Uchaker, S. Candelaria, L. Shen, T. Wang and G. Cao, *Nano Energy*, 2013, **2**, 769–778.
26 A. E. Fischer, K. A. Pettigrew, D. R. Rolison, R. M. Stroud and J. W. Long, *Nano Lett.*, 2007, **7**, 281–286.
27 A. Pan, D. Liu, X. Zhou, B. B. Garcia, S. Liang, J. Liu and G. Cao, *J. Power Sources*, 2010, **195**, 3893–3899.
28 Y. Qiu, K. Yan and S. Yang, *Chem. Commun.*, 2010, **46**, 8359–8361.
29 H.-X. Zhang, C. Feng, Y.-C. Zhai, K.-L. Jiang, Q.-Q. Li and S.-S. Fan, *Adv. Mater.*, 2009, **21**, 2299–2304.
30 Z. Dong, S. J. Kennedy and Y. Wu, *J. Power Sources*, 2011, **196**, 4886–4904.
31 P. Wang, D. Zhang, F. Ma, Y. Ou, Q. N. Chen, S. Xie and J. Li, *Nanoscale*, 2012, **4**, 7199–7204.
32 B. Wang, T. Zhu, H. B. Wu, R. Xu, J. S. Chen and X. W. Lou, *Nanoscale*, 2012, **4**, 2145–2149.
33 L. Wang, Y. Yu, P. C. Chen, D. W. Zhang and C. H. Chen, *J. Power Sources*, 2008, **183**, 717–723.
34 L. Ji, Z. Lin, A. J. Medford and X. Zhang, *Chem.–Eur. J.*, 2009, **15**, 10718–10722.
35 C. V. Schenck, J. G. Dillard and J. W. Murray, *J. Colloid Interface Sci.*, 1983, **95**, 398–409.
36 R. Dedryvère, S. Laruelle, S. Grugeon, P. Poizot, D. Gonbeau and J. M. Tarascon, *Chem. Mater.*, 2004, **16**, 1056–1061.
37 Z.-S. Wu, W. Ren, L. Wen, L. Gao, J. Zhao, Z. Chen, G. Zhou, F. Li and H.-M. Cheng, *ACS Nano*, 2010, **4**, 3187–3194.
38 D. Barreca, C. Massignan, S. Daolio, M. Fabrizio, C. Piccirillo, L. Armelao and E. Tondello, *Chem. Mater.*, 2001, **13**, 588–593.
39 L. Fu, Z. Liu, Y. Liu, B. Han, P. Hu, L. Cao and D. Zhu, *Adv. Mater.*, 2005, **17**, 217–221.
40 B. Varghese, C. H. Teo, Y. Zhu, M. V. Reddy, B. V. R. Chowdari, A. T. S. Wee, V. B. C. Tan, C. T. Lim and C. H. Sow, *Adv. Funct. Mater.*, 2007, **17**, 1932–1939.
41 Y. Wu, S. Fang and Y. Jiang, *Solid State Ionics*, 1999, **120**, 117–123.
42 Y. P. Wu, C. Y. Jiang, C. R. Wan, S. B. Fang and Y. Y. Jiang, *J. Appl. Polym. Sci.*, 2000, **77**, 1735–1741.
43 J.-H. Zhou, Z.-J. Sui, J. Zhu, P. Li, D. Chen, Y.-C. Dai and W.-K. Yuan, *Carbon*, 2007, **45**, 785–796.
44 C.-W. Tang, C.-B. Wang and S.-H. Chien, *Thermochim. Acta*, 2008, **473**, 68–73.
45 H. Guan, C. Shao, S. Wen, B. Chen, J. Gong and X. Yang, *Mater. Chem. Phys.*, 2003, **82**, 1002–1006.
46 N. A. M. Barakat, M. S. Khil, F. A. Sheikh and H. Y. Kim, *J. Phys. Chem. C*, 2008, **112**, 12225–12233.
47 Y. Ding, P. Zhang, Z. Long, Y. Jiang, J. Huang, W. Yan and G. Liu, *Mater. Lett.*, 2008, **62**, 3410–3412.
48 J. Jiang, J. Liu, R. Ding, X. Ji, Y. Hu, X. Li, A. Hu, F. Wu, Z. Zhu and X. Huang, *J. Phys. Chem. C*, 2009, **114**, 929–932.
49 L. W. Ji and X. W. Zhang, *Nanotechnology*, 2009, **20**, 155705.
50 H.-J. Liu, S.-H. Bo, W.-J. Cui, F. Li, C.-X. Wang and Y.-Y. Xia, *Electrochim. Acta*, 2008, **53**, 6497–6503.
51 X. D. Yan, D. H. Min, L. W. Zhao, G. E. Q. Jie, Y. C. Ying and X. H. Yong, *Chemical Journal of Chinese University*, 2006, **27**, 1746–1748.
52 Y. Wang, S. Serrano and J. Santiago-Aviles, *J. Mater. Sci. Lett.*, 2002, **21**, 1055–1057.
53 L. Zou, L. Gan, F. Kang, M. Wang, W. Shen and Z. Huang, *J. Power Sources*, 2010, **195**, 1216–1220.
54 B. Wang, J. Cheng, Y. Wu, D. Wang and D. He, *J. Mater. Chem. A*, 2013, **1**, 1368–1373.